Rapid Communications

Evidence of nodal gap structure in the basal plane of the FeSe superconductor

Pabitra K. Biswas,[1,*] Andreas Kreisel,[2] Qisi Wang,[3] Devashibhai T. Adroja,[1,4] Adrian D. Hillier,[1] Jun Zhao,[3] Rustem Khasanov,[5] Jean-Christophe Orain,[5] Alex Amato,[5] and Elvezio Morenzoni[5]

[1]*ISIS Pulsed Neutron and Muon Source, STFC Rutherford Appleton Laboratory, Harwell Campus, Didcot, Oxfordshire OX11 0QX, United Kingdom*

[2]*Institut für Theoretische Physik, Universität Leipzig, D-04103 Leipzig, Germany*

[3]*State Key Laboratory of Surface Physics and Department of Physics, Fudan University, Shanghai 200433, China*

[4]*Highly Correlated Matter Research Group, Physics Department, University of Johannesburg, P.O. Box 524, Auckland Park 2006, South Africa*

[5]*Laboratory for Muon Spin Spectroscopy, Paul Scherrer Institut, CH-5232 Villigen PSI, Switzerland*

(Received 26 April 2018; revised manuscript received 12 September 2018; published 8 November 2018)

Identifying the symmetry of the wave function describing the Cooper pairs is pivotal in understanding the origin of high-temperature superconductivity in iron-based superconductors. Despite nearly a decade of intense investigation, the answer to this question remains elusive. Here, we use the muon spin rotation/relaxation (μSR) technique to investigate the underlying symmetry of the pairing state of the FeSe superconductor, the basic building block of all iron-chalcogenide superconductors. Contrary to earlier μSR studies on powders and crystals, we show that while the superconducting gap is most probably anisotropic but nodeless along the crystallographic c axis, it is nodal in the ab plane, as indicated by the linear increase of the superfluid density at low temperature. We further show that the superconducting properties of FeSe display a less pronounced anisotropy than expected.

DOI: 10.1103/PhysRevB.98.180501

High-transition-temperature T_c superconductivity in Fe-based materials is an intriguing emergent phenomenon in modern condensed matter physics research [1–5]. Among various Fe-based superconductors, FeSe is one of the most interesting and intensively studied compounds due to its extremely simple crystal structure, high T_c values, unconventional superconducting state, and unusual normal-state properties. Superconductivity takes place in the FeSe layer which is the basic building block of all Fe-chalcogenide superconductors [6]. Despite nearly a decade of extensive research, the symmetry of the superconducting gaps in FeSe, which is intimately connected to the electron pairing mechanism in this material and all other related Fe-based superconductors, is still the subject of intense debate. While anisotropic line nodes or deep minima in the superconducting gaps have been suggested theoretically in FeSe [7], most experimental techniques have detected two superconducting gaps, however, without any consensus about the presence or absence of nodes in either of the gaps [8–17]. Notable exceptions are surface-sensitive scanning tunneling spectroscopic (STS) measurements performed on FeSe thin films, which detected V-shaped conducting spectra in the superconducting state, indicating the presence of nodes in the gap structure [18]. A similar STS experiment conducted on the twin boundaries of FeSe single crystals displayed a fully gapped structure, suggesting a gap-symmetry evolution from nodal in the bulk to nodeless at the twin boundaries [19], a finding that has been argued to be in agreement with the detection of a finite gap in multiple domains while in single domains the gap is found to be zero within experimental resolution [20]. Recently, Sprau *et al.* used a quasiparticle interference imaging technique and detected gap minima in the α and ϵ bands of the Fe plane [21]. They further suggested that the Cooper pairing in FeSe is orbital selective, involving predominantly the d_{yz} orbitals of the Fe atoms. However, the majority of the techniques used so far in detecting nodes or gap minima are surface sensitive only and give limited or no information about the symmetry of the pairing state in the bulk of FeSe. To date, there is no clear and direct bulk evidence of nodes in the gap structure of FeSe. Clarifying this issue is highly desirable not only to determine the exact nature of the superconducting state in FeSe, but also because a comparison with the other Fe-based superconductors and the cuprates may pave the way to understand the essential ingredients of high-temperature superconductivity.

In this Rapid Communication, we have used the muon spin rotation/relaxation (μSR) technique to reveal the symmetry of the superconducting gap along the crystallographic c axis and ab plane of FeSe single crystals. The measurement of the field distribution in the vortex state by μSR is one of the most direct and accurate methods to determine the absolute value of the magnetic penetration depth λ and its temperature dependence [22]. $\lambda(T)$ is related to the effective superfluid density, the density of the superconducting carriers n_s, as $\lambda^{-2}(T) \propto \frac{n_s(T)}{m^*}$, where m^* is the effective mass. The low-temperature behavior of $\lambda(T)$ directly reflects the low-energy properties of the quasiparticle spectrum, and is therefore sensitive to the presence or absence of nodes in the superconducting gap. While for a fully gapped s-wave superconductor

*pabitra.biswas@stfc.ac.uk

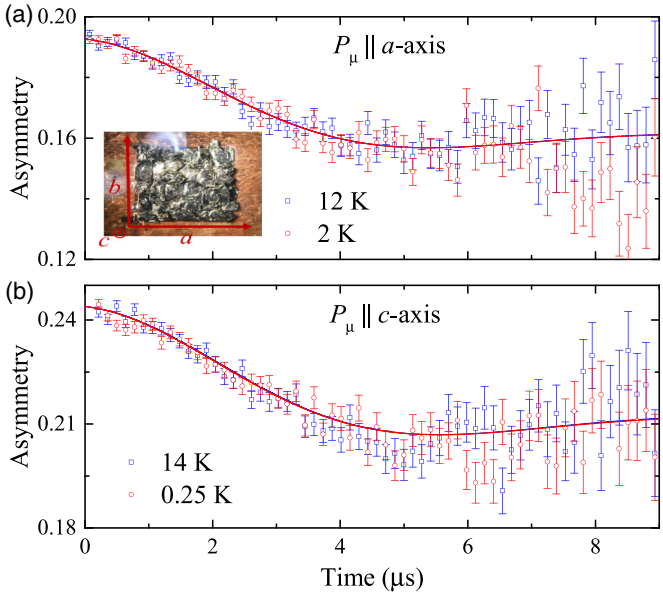

FIG. 1. ZF-μSR time spectra, collected above and below T_c with muon spin polarization P_μ parallel to the (a) a axis and (b) c axis. The solid lines are the fits to the data using the Kubo-Toyabe Gaussian distribution function, described in the text. The inset in (a) shows the mosaic of the aligned FeSe crystals used in this study.

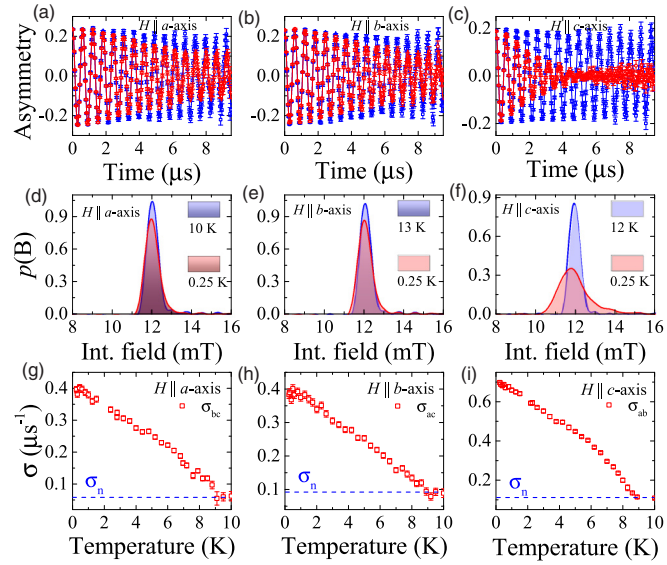

FIG. 2. (a)–(c) TF-μSR time spectra of FeSe, collected above and below T_c in a TF of 12 mT applied parallel to the a, b, and c axis, respectively. The solid lines are the fit to the data using a sum of Gaussian field distributions, described in the text. (d)–(f) Fast Fourier transformation of the TF-μSR spectra, showing the line shape of the internal fields along all three crystallographic axes. (g)–(i) Temperature dependence of the muon spin damping rate σ along three crystallographic directions, extracted from the TF-μSR time spectra. The dashed horizontal lines represent the normal-state contribution σ_n.

$\lambda^{-2}(T)$ saturates exponentially with decreasing temperature, it increases linearly in a nodal superconductor [22]. Here, we report the direct observation of nodal superconductivity in the basal plane of FeSe. We show that while the temperature dependence of the superfluid density along the crystallographic c axis is compatible with either a nodeless anisotropic s-wave or isotropic two-gap $s + s$-wave symmetries, that in the basal ab plane is better fitted assuming a two-gap $s + d$-wave symmetry. The nodal d-wave component reflects the linear increase of the superfluid density with decreasing temperature close to $T = 0$. The transition of the pairing symmetry from nodeless to nodal, as we probe from the *out-of-plane* to the *in-plane* direction in the FeSe layer, suggests a directional-dependent pairing symmetry in FeSe.

The sample used in these experiments was a 1-cm^2 mosaic of around 30 single crystals, all of them carefully aligned along the three nominal crystallographic axes a, b, and c. Details about the crystal growth are described in Ref. [23]. The crystals were mounted on a 50-μm-thin copper foil, attached to a fork-shaped copper sample holder [see Fig. 1(a), inset]. Zero-field (ZF) and transverse-field (TF) μSR experiments were carried out using coaligned crystals. Figures 1(a) and 1(b) show the typical ZF-μSR time spectra collected above and below T_c with muon spin polarization P_μ parallel to the crystallographic a and b axis. The solid lines are the fits to the data using the Kubo-Toyabe Gaussian distribution function, which describes the temporal evolution of the spin polarization in the presence of randomly oriented nuclear moments [24]. Details are described in the Supplemental Material (SM) [25]. ZF data collected above and below T_c in both orientations do not show any detectable additional relaxation in the asymmetry spectra, therefore completely ruling out the presence of any magnetism in the superconducting state of FeSe.

Three sets of TF-μSR experiments were performed with the magnetic field H applied parallel to three crystallographic axes. Figures 2(a)–2(c) show the TF-μSR asymmetry spectra collected above and below T_c with $H = 12$ mT applied along the nominal a, b, and c axis, respectively. As expected, the TF-μSR signals decay much faster in the superconducting state than in the normal state due to the formation of a vortex lattice and the associated inhomogeneous magnetic field distribution. Figures 2(d)–2(f) show the fast Fourier transformation (FFT) of the TF-μSR spectra, revealing the line shape of the internal magnetic field distributions $p(B)$ probed by the muons. Both TF-μSR time spectra and corresponding FFT clearly demonstrate that the μSR responses are identical for H applied parallel to the nominal a and b axis. This is expected due to the formation of structural twin domains in FeSe crystals. The background signal is relatively large for H applied parallel to the a and b axis. This is due to the bending of the muon beam under transverse magnetic field to the muon momentum. The field distribution in the FFT signals shows that $p(B)$ is much more asymmetric for the $H \parallel c$ axis than the $H \parallel a/b$ axis. Also, the damping of the TF-μSR signals in the superconducting state is much stronger for the $H \parallel c$ axis than the $H \parallel a/b$ axis.

The muon spin depolarization rate σ can be determined by fitting the TF-μSR asymmetry spectra collected with the $H \parallel a/b$ axis using damped spin precession functions

$$A_{\mathrm{TF}}(t) = A_0 \exp(-\sigma^2 t^2/2)\cos(\gamma_\mu \langle B\rangle t + \phi) + A_{\mathrm{bg}} \cos(\gamma_\mu B_{\mathrm{bg}} t + \phi), \quad (1)$$

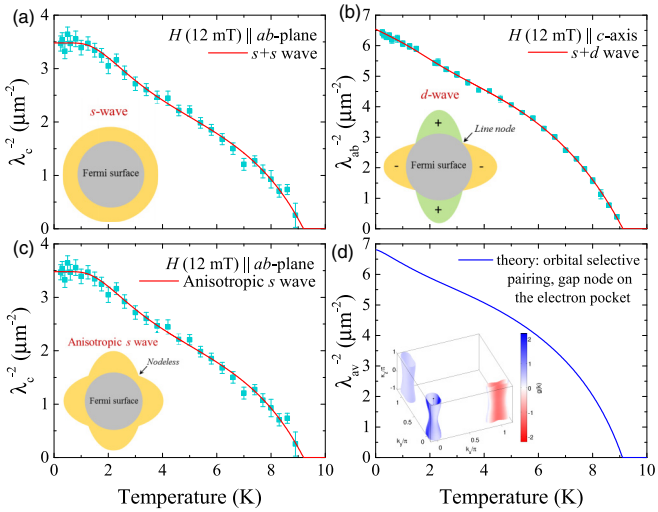

FIG. 3. (a), (c) Temperature dependence of λ^{-2} for FeSe along the crystallographic c axis. The solid curves are the fit to the $\lambda_c^{-2}(T)$ using a nodeless anisotropic s-wave and two-gap $s+s$-wave models. (b) Temperature dependence of λ^{-2} for FeSe in the ab plane. The solid curves is the fit to the $\lambda_{ab}^{-2}(T)$ using a two-gap $s+d$-wave model. (d) Calculation of the averaged penetration depth $\lambda_{\rm av}^{-2}$ from a microscopic model for the order parameter and the electronic structure. The insets are the schematic of the isotropic s-, anisotropic s-, and d-wave-type gap symmetries around the Fermi surface and the gap structure for the microscopic model in (d).

where A_0 and $A_{\rm bg}$ are the initial asymmetries of the sample and background signals, respectively, $\gamma_\mu/2\pi = 135.5$ MHz/T is the muon gyromagnetic ratio [22], $\langle B\rangle$ and $B_{\rm bg}$ are the internal and background magnetic fields, and ϕ is the initial phase of the muon precession signal. In order to account for the highly asymmetric nature of $p(B)$, TF-μSR asymmetry spectra collected for H applied parallel to the c axis were analyzed using the skewed Gaussian (SKG) field distribution, as described in Ref. [26] (also see SM).

Figures 2(g)–2(i) show the temperature dependence of σ along all three crystallographic directions, extracted from the TF-μSR time spectra. The depolarization rate can be expressed as the geometric mean of the superconducting contribution to the relaxation rate due to the inhomogeneous field distributions of the vortex lattice $\sigma_{\rm sc}$ and the temperature-independent nuclear magnetic dipolar contribution $\sigma_{\rm nm}$, i.e., $\sigma = \sqrt{\sigma_{\rm sc}^2 + \sigma_{\rm nm}^2}$.

The temperature dependence of the *in-plane* and *out-of-plane* components of the magnetic penetration depth λ_{ab} and λ_c were calculated from $\sigma_{\rm sc}^{\|a}$, $\sigma_{\rm sc}^{\|b}$, and $\sigma_{\rm sc}^{\|c}$ by using the simplified Brandt equation [26,27], as described in Ref. [26] (also see SM). Figures 3(a)–3(c) show the temperature dependence of λ^{-2} for FeSe along the crystallographic c axis and ab plane, respectively. The solid curves are the fit to the $\lambda^{-2}(T)$ using either a single-gap or a two-gap model,

$$\frac{\lambda^{-2}(T)}{\lambda^{-2}(0)} = \omega\frac{\lambda^{-2}(T,\Delta_{0,1})}{\lambda^{-2}(0,\Delta_{0,1})} + (1-\omega)\frac{\lambda^{-2}(T,\Delta_{0,2})}{\lambda^{-2}(0,\Delta_{0,2})}. \quad (2)$$

Here, $\lambda(0)$ is the value of the penetration depth at $T = 0$ K, $\Delta_{0,i}$ is the value of the ith ($i = 1$ or 2) superconducting gap at $T = 0$ K, and ω is the weighting factor of the first gap.

TABLE I. Fitted parameters to the $\lambda_{ab}^{-2}(T)$ and $\lambda_c^{-2}(T)$ data of FeSe using the different models described in the text.

Data	Model	Gap value (meV)	$\lambda(0)$ (nm)	$\chi^2_{\rm reduced}$
$\frac{1}{\lambda_{ab}^2(T)}$	s wave	$\Delta = 1.22(1)$		39.56
	d wave	$\Delta = 1.99(2)$		4.39
	Anisotropic s wave	$\Delta = 1.40(2)$, $a = 0.81(2)$, with $\Delta_{\rm max} = 2.53(4)$		1.48
	$s+s$ wave	$\Delta_1 = 1.75(6)$, $\Delta_2 = 0.40(3)$, and $\omega = 0.68(6)$		1.40
	$s+d$ wave	$\Delta_1 = 1.86(8)$, $\Delta_2 = 0.73(8)$, and $\omega = 0.60(2)$	391(16)	1.01
$\frac{1}{\lambda_c^2(T)}$	s wave	$\Delta = 1.19(3)$		8.41
	d wave	$\Delta = 1.9(1)$		4.35
	Anisotropic s wave	$\Delta = 1.28(4)$, $a = 0.76(4)$, with $\Delta_{\rm max} = 2.3(1)$	514(53)	1.50
	$s+s$ wave	$\Delta_1 = 2.2(3)$, $\Delta_2 = 0.6(1)$, and $\omega = 0.48(7)$		1.51
	$s+d$ wave	$\Delta_1 = 1.8(1)$, $\Delta_2 = 1.0(1)$, and $\omega = 0.44(1)$		1.81

Each term in Eq. (2) is evaluated using the standard expression within the local London approximation ($\lambda \gg \xi$) [28] as

$$\frac{\lambda^{-2}(T,\Delta_{0,i})}{\lambda^{-2}(0,\Delta_{0,i})} = 1 + \frac{1}{\pi}\int_0^{2\pi}\int_{\Delta_{(T,\varphi)}}^{\infty}\frac{\left(\frac{\partial f}{\partial E}\right)E\,dE\,d\varphi}{\sqrt{E^2-\Delta_i^2(T,\varphi)}}, \quad (3)$$

where $f = [1+\exp(E/k_{\rm B}T)]^{-1}$ is the Fermi function, φ is the angle along the Fermi surface, and $\Delta_i(T,\varphi) = \Delta_{0,i}\delta(T/T_c)g(\varphi)$, where $g(\varphi)$ describes the angular dependence of the gap. $g(\varphi)$ is 1 for the s-wave and $s+s$-wave gaps, $|\cos(2\varphi)|$ for a d wave, and $[1+a|\cos(4\varphi)|]$ for an anisotropic s-wave gap. An approximation to the temperature dependence in $\Delta(T)$ can be written as $\delta(T/T_c) = \tanh\{1.82[1.018(T_c/T-1)]^{0.51}\}$ [29].

All the fitted parameters are summarized in Table I and details about the fit functions are described in the SM. For the superfluid density along the c axis, i.e., $1/\lambda_c^2(T)$ ($H||ab$ plane), both the single-gap anisotropic s-wave and two-gap $s+s$-wave gap models give the lowest $\chi^2_{\rm reduced}$ value and hence represent the best fit to the data compared to any other models tried here. Gap parameters extracted from analysis are in excellent agreement with most of the reported values obtained on this system [8–15,20].

For the superfluid density in the ab plane, i.e., $1/\lambda_{ab}^2(T)$ ($H||c$ axis), we need to introduce a nodal d-wave gap along with an isotropic s-wave gap in order to reproduce the linear increase of the superfluid density close to zero temperature. We find that the $s+d$-wave model gives a much lower $\chi^2_{\rm reduced}$ value than others. Our results strongly suggest that FeSe is indeed a multigap superconductor. The experimentally obtained superfluid density in the basal plane shows properties of a nodal superconductor irrespective of the field direction. These findings differ qualitatively from earlier reports on the μSR studies of FeSe evidencing nodeless superconductivity in this material [8,10]. This is probably due to the use of

polycrystalline samples which is expected to give an average effect from all three directions. It is also well known that the presence of impurities can sometimes mask the true nature of the superconducting gap [30]. Our results are also consistent with the STS measurements performed on FeSe thin films showing nodes in the gap structure [18]. Recent specific heat data collected on the single crystals of FeSe show a linear behavior at low temperature, a signature that has been interpreted as nodal superconductivity [31,32]. More recently, Sun *et al.* has performed field-angle-resolved specific heat measurements of FeSe and found three superconducting gaps in FeSe with line nodes in the smaller gap [33]. A strongly anisotropic gap structure with deep minima has been observed in recent quasiparticle interference (QPI) imaging measurements by Sprau *et al.* [21]. An anisotropic gap structure has also been found along all momentum directions in a recent angle-resolved photoemission spectroscopy (ARPES) measurements by Kushnirenko *et al.* [34]. It is important to note here that both QPI imaging and ARPES are surface-sensitive techniques and the deep minima observed at the surface may become nodes in the bulk of the FeSe superconductor.

To draw conclusions from the measured in-plane and out-of-plane penetration depths beyond the general statement of the presence or absence of nodal behavior in certain directions, we also present microscopic calculations of the penetration depth. For this purpose, we start from a recently proposed model for the electronic structure with the eigenenergies $\tilde{E}_\mu(\mathbf{k})$ that is consistent with a number of experimental investigations on FeSe [21,35]. The superconducting gap function has been slightly modified to introduce a nodal structure in the bulk of FeSe. Taking into account the electronic structure as being a correlated electron gas via a reduced quasiparticle weight, one can calculate the penetration depth (tensor) without any free parameters. The key ingredient is the parametrization of the Green's function for band ν in presence of correlations via $\tilde{G}_\nu(\mathbf{k},\omega_n) = \tilde{Z}_\nu(\mathbf{k})[i\omega_n - \tilde{E}_\mu(\mathbf{k})]^{-1}$, where $\tilde{Z}_\nu(\mathbf{k}) = [\sum_s |a_\nu^s(\mathbf{k})|^2\sqrt{Z_s}]^2$ is the momentum-dependent quasiparticle weight that is obtained from the quasiparticle weights of the orbitals Z_s and the matrix elements $a_\nu^s(\mathbf{k})$ for the orbital-to-band transformation [21,35]. The structure of the matrix elements and the values of the quasiparticle weights have been deduced earlier [21,35]. Details on the calculation of the inverse square of penetration depth λ_i^{-2} for shielding supercurrent flowing in the i direction are presented in the Supplemental Material [25]. At the moment, we simply ignore the contribution of one of the Fermi surface pockets (δ pocket) to the penetration depth. In line with the previous theoretical considerations and also in accordance to the expectations of the principal axis of the superfluid tensor [18], we choose the direction of the short Fe-Fe bond, the long Fe-Fe bond, and the crystallographic c axis as directions of our calculations. Noting that the relative magnitudes of λ_x and λ_y agree with the observed orientation of elongated vortices in FeSe (see SM), we need to keep in mind that the present experiment does not see the difference between the two directions because of the twinning of the crystals. The geometric mean of the penetration depth in the plane $\lambda_{\rm av}$ is equivalent to the measured averaged penetration depth λ_{ab} due to the tensor nature of the superfluid density [36] (see SM). In Fig. 3(d) we show the result for $\lambda_{\rm av}$ from this calculation. From a theoretical point of view, the full gap is not robust against node formation, because FeSe in the nematic state allows spherical harmonics from s-wave-type gap functions to superimpose to contributions of d-wave symmetry, thus the relative strength of these contributions determines on whether the order parameter goes to zero on the Fermi surface. The properties of the pairing interaction and thus the superconducting gap can be slightly modified on the surface. Thus our result does not contradict the experimental findings by QPI [21]. Therefore, we used a gap function exhibiting nodes on the electron pocket [see Fig. 3(d), inset]. It is evident that the mentioned fully gapped state yields a saturating superfluid density at low temperatures, while the nodal state produces linear behavior in that quantity. A direct comparison of the calculated and measured penetration depth λ^{-2} over the full temperature range reveals only a difference of 5% from the experimentally deduced value, an error that can easily be explained by errors in the gap magnitude and the Fermi velocities (see SM).

Table I shows the absolute values of the penetration depth $\lambda(0)$ in both directions. In the basal plane $\lambda(0)$ is 391(16) nm, which is lower than the value 514(53) nm out of the basal plane and reflects the anisotropic superconducting properties in FeSe. Theoretically, a much larger value of λ_c is expected given the small dispersion of the proposed electronic structure and the small Fermi velocities in the k_z direction. Even when taking into account a possible misalignment of the external field, our results indicate a more three-dimensional electronic structure for FeSe. From our determination of $\lambda(0)$ and using the reported value of effective mass $m^* \approx 4m_e$ [37] in the expression for the density of paired electrons $n_s(0) = \frac{m^*}{\mu_0 e^2 \lambda^2(0)}$, we estimate $n_s^{\parallel ab}(0) \approx 7.4 \times 10^{20}$ cm^{-3} and $n_s^{\parallel c}(0) \approx 3.9 \times 10^{20}$ cm^{-3}. These values show that the overall carrier density in FeSe is small, with the basal plane of FeSe playing a preferred role in carrying superconductivity.

The observation of line nodes in the basal plane of FeSe superconductor is the main finding of this Rapid Communication. This conclusion does not require a specific theoretical model, but is directly related to the observed low-temperature behavior of $1/\lambda^2(T)$, which shows saturation in the out of plane and a linear increase in the basal plane as the temperature decreases to absolute zero. Such a linear increase of superfluid density reflects the presence of low-energy excitations and thus confirms nodes in the superconducting gap structure of FeSe.

D.T.A. would like to thank the Royal Society of London for U.K.-China Newton funding. Q.W. and J.Z. were supported by the National Natural Science Foundation of China (Grant No. 11374059), the National Key R&D Program of the MOST of China (Grant No. 2016YFA0300203), and the Ministry of Science and Technology of China (Program 973: 2015CB921302). Data are available from the corresponding author upon request.

[1] J. Paglione and R. L. Greene, High-temperature superconductivity in iron-based materials, Nat. Phys. **6**, 645 (2010).

[2] G. R. Stewart, Superconductivity in iron compounds, Rev. Mod. Phys. **83**, 1589 (2011).

[3] F. Wang and D.-H. Lee, The electron-pairing mechanism of iron-based superconductors, Science **332**, 200 (2011).

[4] H.-H. Wen and S. Li, Materials and novel superconductivity in iron pnictide superconductors, Annu. Rev. Condens. Matter Phys. **2**, 121 (2011).

[5] A. Chubukov and P. J. Hirschfeld, Iron-based superconductors, seven years later, Phys. Today **68**(6), 46 (2015).

[6] A. E. Böhmer and A. Kreisel, Nematicity, magnetism and superconductivity in FeSe, J. Phys.: Condens. Matter **30**, 023001 (2018).

[7] S. Mukherjee, A. Kreisel, P. J. Hirschfeld, and B. M. Andersen, Model of Electronic Structure and Superconductivity in Orbitally Ordered FeSe, Phys. Rev. Lett. **115**, 026402 (2015).

[8] R. Khasanov, K. Conder, E. Pomjakushina, A. Amato, C. Baines, Z. Bukowski, J. Karpinski, S. Katrych, H.-H. Klauss, H. Luetkens, A. Shengelaya, and N. D. Zhigadlo, Evidence of nodeless superconductivity in $FeSe_{0.85}$ from a muon-spin-rotation study of the in-plane magnetic penetration depth, Phys. Rev. B **78**, 220510 (2008).

[9] J. K. Dong, T. Y. Guan, S. Y. Zhou, X. Qiu, L. Ding, C. Zhang, U. Patel, Z. L. Xiao, and S. Y. Li, Multigap nodeless superconductivity in $FeSe_x$: Evidence from quasiparticle heat transport, Phys. Rev. B **80**, 024518 (2009).

[10] R. Khasanov, M. Bendele, A. Amato, K. Conder, H. Keller, H.-H. Klauss, H. Luetkens, and E. Pomjakushina, Evolution of Two-Gap Behavior of the Superconductor $FeSe_{1-x}$, Phys. Rev. Lett. **104**, 087004 (2010).

[11] Ya. G. Ponomarev, S. A. Kuzmichev, M. G. Mikheev, M. V. Sudakova, S. N. Tchesnokov, T. E. Shanygina, O. S. Volkova, A. N. Vasiliev, and Th. Wolf, Andreev spectroscopy of FeSe: Evidence for two-gap superconductivity, J. Exp. Theor. Phys. **113**, 459 (2011).

[12] J.-Y. Lin, Y. S. Hsieh, D. A. Chareev, A. N. Vasiliev, Y. Parsons, and H. D. Yang, Coexistence of isotropic and extended s-wave order parameters in FeSe as revealed by low-temperature specific heat, Phys. Rev. B **84**, 220507 (2011).

[13] M. Abdel-Hafiez, J. Ge, A. N. Vasiliev, D. A. Chareev, J. Van de Vondel, V. V. Moshchalkov, and A. V. Silhanek, Temperature dependence of lower critical field $H_{c1}(T)$ shows nodeless superconductivity in FeSe, Phys. Rev. B **88**, 174512 (2013).

[14] S. Kasahara, T. Watashige, T. Hanaguri, Y. Kohsaka, T. Yamashita, Y. Shimoyama, Y. Mizukami, R. Endo, H. Ikeda, K. Aoyama, T. Terashima, S. Uji, T. Wolf, H. von Löhneysen, T. Shibauchi, and Y. Matsuda, Field-induced superconducting phase of FeSe in the BCS-BEC cross-over, Proc. Natl. Acad. Sci. USA **111**, 16309 (2014).

[15] P. Bourgeois-Hope, S. Chi, D. A. Bonn, R. Liang, W. N. Hardy, T. Wolf, C. Meingast, N. Doiron-Leyraud, and L. Taillefer, Thermal Conductivity of the Iron-Based Superconductor FeSe: Nodeless Gap with a Strong Two-Band Character, Phys. Rev. Lett. **117**, 097003 (2016).

[16] T. Watashige, S. Arsenijević, T. Yamashita, D. Terazawa, T. Onishi, L. Opherden, S. Kasahara, Y. Tokiwa, Y. Kasahara, T. Shibauchi, H. von Löhneysen, J. Wosnitza, and Y. Matsuda, Quasiparticle excitations in the superconducting state of FeSe probed by thermal Hall conductivity in the vicinity of the BCS-BEC crossover, J. Phys. Soc. Jpn. **86**, 014707 (2017).

[17] M. Li, N. R. Lee-Hone, S. Chi, R. Liang, W. N. Hardy, D. A. Bonn, E. Girt, and D. M. Broun, Superfluid density and microwave conductivity of FeSe superconductor: ultralong-lived quasiparticles and extended s-wave energy gap, New J. Phys. **18**, 082001 (2016).

[18] C.-L. Song, Y.-L. Wang, P. Cheng, Y.-P. Jiang, W. Li, T. Zhang, Z. Li, K. He, L. Wang, J.-F. Jia, H.-H. Hung, C. Wu, X. Ma, X. Chen, and Q.-K. Xue, Direct observation of nodes and twofold symmetry in FeSe superconductor, Science **332**, 1410 (2011).

[19] T. Watashige, Y. Tsutsumi, T. Hanaguri, Y. Kohsaka, S. Kasahara, A. Furusaki, M. Sigrist, C. Meingast, T. Wolf, H. v. Löhneysen, T. Shibauchi, and Y. Matsuda, Evidence for Time-Reversal Symmetry Breaking of the Superconducting State Near Twin-Boundary Interfaces in FeSe Revealed by Scanning Tunneling Spectroscopy, Phys. Rev. X **5**, 031022 (2015).

[20] T. Hashimoto, Y. Ota, H. Q. Yamamoto, Y. Suzuki, T. Shimojima, S. Watanabe, C. Chen, S. Kasahara, Y. Matsuda, T. Shibauchi, K. Okazaki, and S. Shin, Superconducting gap anisotropy sensitive to nematic domains in FeSe, Nat. Commun. **9**, 282 (2018).

[21] P. O. Sprau, A. Kostin, A. Kreisel, A. E. Böhmer, V. Taufour, P. C. Canfield, S. Mukherjee, P. J. Hirschfeld, B. M. Andersen, and J. C. Séamus Davis, Discovery of orbital-selective cooper pairing in FeSe, Science **357**, 75 (2017).

[22] J. E. Sonier, J. H. Brewer, and R. F. Kiefl, μSR studies of the vortex state in type-II superconductors, Rev. Mod. Phys. **72**, 769 (2000).

[23] Q. Wang, Y. Shen, B. Pan, X. Zhang, K. Ikeuchi, K. Iida, A. D. Christianson, H. C. Walker, D. T. Adroja, M. Abdel-Hafiez, X. Chen, D. A. Chareev, A. N. Vasiliev, and J. Zhao, Magnetic ground state of FeSe, Nat. Commun. **7**, 12182 (2016).

[24] R. Kubo, A stochastic theory of spin relaxation, Hyperfine Interact. **8**, 731 (1981).

[25] See Supplemental Material at http://link.aps.org/supplemental/10.1103/PhysRevB.98.180501 for the characterization measurements of the FeSe single crystals using a superconducting quantum interference device (SQUID) magnetometer, details about the experimental methods and data analysis, and a summary of the theoretical modeling and calculations that otherwise need to be looked up from various references, which includes Refs. [38–49].

[26] R. Khasanov, H. Zhou, A. Amato, Z. Guguchia, E. Morenzoni, X. Dong, G. Zhang, and Z. Zhao, Proximity-induced superconductivity within the insulating $(Li_{0.84}Fe_{0.16})OH$ layers in $(Li_{0.84}Fe_{0.16})OHFe_{0.98}Se$, Phys. Rev. B **93**, 224512 (2016).

[27] E. H. Brandt, Flux distribution and penetration depth measured by muon spin rotation in high-T_c superconductors, Phys. Rev. B **37**, 2349 (1988).

[28] R. Prozorov and R. W. Giannetta, Magnetic penetration depth in unconventional superconductors, Supercond. Sci. Technol. **19**, R41 (2006).

[29] A. Carrington and F. Manzano, Magnetic penetration depth of MgB_2, Physica C **385**, 205 (2003).

[30] J. E. Sonier, J. H. Brewer, R. F. Kiefl, G. D. Morris, R. I. Miller, D. A. Bonn, J. Chakhalian, R. H. Heffner, W. N. Hardy, and R. Liang, Field Induced Reduction of the Low-Temperature Superfluid Density in $YBa_2Cu_3O_{6.95}$, Phys. Rev. Lett. **83**, 4156 (1999).

[31] L. Jiao, C.-L. Huang, S. Rößler, C. Koz, U.K. Rößler, U. Schwarz, and S. Wirth, Superconducting gap structure of FeSe, Sci. Rep. **7**, 44024 (2017).

[32] F. Hardy, M. He, L. Wang, T. Wolf, P. Schweiss, M. Merz, M. Barth, P. Adelmann, R. Eder, A.-A. Haghighirad, and C. Meingast, Nodal gaps in the nematic superconductor FeSe from heat capacity, arXiv:1807.07907.

[33] Y. Sun, S. Kittaka, S. Nakamura, T. Sakakibara, K. Irie, T. Nomoto, K. Machida, J. Chen, and T. Tamegai, Gap structure of FeSe determined by angle-resolved specific heat measurements in applied rotating magnetic field, Phys. Rev. B **96**, 220505 (2017).

[34] Y. S. Kushnirenko, A. V. Fedorov, E. Haubold, S. Thirupathaiah, T. Wolf, S. Aswartham, I. Morozov, T. K. Kim, B. Büchner, and S. V. Borisenko, Three-dimensional superconducting gap in FeSe from angle-resolved photoemission spectroscopy, Phys. Rev. B **97**, 180501 (2018).

[35] A. Kreisel, B. M. Andersen, P. O. Sprau, A. Kostin, J. C. S. Davis, and P. J. Hirschfeld, Orbital selective pairing and gap structures of iron-based superconductors, Phys. Rev. B **95**, 174504 (2017).

[36] S. L. Thiemann, Z. Radović, and V. G. Kogan, Field structure of vortex lattices in uniaxial superconductors, Phys. Rev. B **39**, 11406 (1989).

[37] M. D. Watson, T. K. Kim, A. A. Haghighirad, N. R. Davies, A. McCollam, A. Narayanan, S. F. Blake, Y. L. Chen, S. Ghannadzadeh, A. J. Schofield, M. Hoesch, C. Meingast, T. Wolf, and A. I. Coldea, Emergence of the nematic electronic state in FeSe, Phys. Rev. B **91**, 155106 (2015).

[38] A. Yaouanc and P. Dalmas de Réotier, *Muon Spin Rotation, Relaxation, and Resonance: Applications to Condensed Matter*, International Series of Monographs on Physics No. 147 (Oxford University Press, Oxford, U.K., 2011).

[39] A. Suter and B. M. Wojek, Musrfit: A free platform-independent framework for μSR data analysis, Phys. Proc. **30**, 69 (2012).

[40] A. Maisuradze, R. Khasanov, A. Shengelaya, and H. Keller, Comparison of different methods for analyzing μSR line shapes in the vortex state of type-II superconductors, J. Phys.: Condens. Matter **21**, 075701 (2009).

[41] D. E. Sheehy, T. P. Davis, and M. Franz, Unified theory of the *ab*-plane and *c*-axis penetration depths of underdoped cuprates, Phys. Rev. B **70**, 054510 (2004).

[42] M. V. Eremin, I. A. Larionov, and I. E. Lyubin, London penetration depth in the tight binding approximation: Orthorhombic distortion and oxygen isotope effects in cuprates, J. Phys.: Condens. Matter **22**, 185704 (2010).

[43] L. C. Rhodes, M. D. Watson, A. A. Haghighirad, D. V. Evtushinsky, M. Eschrig, and T. K. Kim, Scaling of the superconducting gap with orbital character in FeSe, arXiv:1804.01436.

[44] L. Benfatto, B. Valenzuela, and L. Fanfarillo, Nematic pairing from orbital-selective spin fluctuations in FeSe, npj Quantum Materials **3**, 56 (2018).

[45] Y. Suzuki, T. Shimojima, T. Sonobe, A. Nakamura, M. Sakano, H. Tsuji, J. Omachi, K. Yoshioka, M. Kuwata-Gonokami, T. Watashige, R. Kobayashi, S. Kasahara, T. Shibauchi, Y. Matsuda, Y. Yamakawa, H. Kontani, and K. Ishizaka, Momentum-dependent sign inversion of orbital order in superconducting FeSe, Phys. Rev. B **92**, 205117 (2015).

[46] M. D. Watson, T. Yamashita, S. Kasahara, W. Knafo, M. Nardone, J. Béard, F. Hardy, A. McCollam, A. Narayanan, S. F. Blake, T. Wolf, A. A. Haghighirad, C. Meingast, A. J. Schofield, H. v. Löhneysen, Y. Matsuda, A. I. Coldea, and T. Shibauchi, Dichotomy between the Hole and Electron Behavior in Multiband Superconductor FeSe Probed by Ultrahigh Magnetic Fields, Phys. Rev. Lett. **115**, 027006 (2015).

[47] M. D. Watson, T. K. Kim, L. C. Rhodes, M. Eschrig, M. Hoesch, A. A. Haghighirad, and A. I. Coldea, Evidence for unidirectional nematic bond ordering in FeSe, Phys. Rev. B **94**, 201107 (2016).

[48] V. G. Kogan, On neutron diffraction from vortices in uniaxial superconductors, Phys. Lett. A **85**, 298 (1981).

[49] L. J. Campbell, M. M. Doria, and V. G. Kogan, Vortex lattice structures in uniaxial superconductors, Phys. Rev. B **38**, 2439 (1988).